Resonant single-photon and multiphoton coherent transitions in a detuned regime

S. Bertaina,[1,*] M. Martens,[2] M. Egels,[1] D. Barakel,[1] and I. Chiorescu[2]
[1]*IM2NP-CNRS (UMR 7334) and Aix-Marseille Université, Faculté des Sciences et Techniques, Avenue Escadrille Normandie Niemen - Case 162, F-13397 Marseille Cedex, France*
[2]*Department of Physics and the National High Magnetic Field Laboratory, Florida State University, Tallahassee, Florida 32310, USA*
(Received 23 April 2015; published 10 July 2015)

We performed quantum manipulations of the multilevel spin system $S = 5/2$ of a Mn^{2+} ion, by means of a two-tone pulse drive. The detuning between the excitation and readout radio frequency pulses allows one to select the number of photons involved in a Rabi oscillation as well as increase the frequency of this nutation. Thus detuning can lead to a resonant multiphoton process. Our analytical model for a two-photon process as well as a numerical generalization fit well the experimental findings, with implications for the use of multilevel spin systems as tunable solid state qubits.

DOI: 10.1103/PhysRevB.92.024408 PACS number(s): 03.67.−a, 71.70.Ch, 75.10.Dg, 76.30.Da

I. INTRODUCTION

Quantum properties of electronic spins can be controlled due to their relatively long coherence times. This is mostly achieved by spin dilution in a nonmagnetic matrix [1–6], leading to coherent Rabi oscillations up to room temperature [1,7]. Fundamental and technological advances can be achieved by strongly coupling spins with photons in a cavity [8–10], leading to a new type of hybrid quantum memory [11]. Recently, we proposed a tunable multilevel system as a potential candidate for multiqubit implementation [6,12] which could be used to implement Grover's algorithm [13–15] for instance. We describe in this work a two-tone experiment using the $S = 5/2$ spin of Mn^{2+} ions diluted in MgO. This technique allows us to study multiphoton dynamics in and out of resonance by detuning the two radio frequencies of the excitation and readout pulses. Interestingly, the detuning can actually be used to bring into resonance levels separated by exactly two or more photons. The implication is that the multilevel electron spin dynamics can now be controlled using any number of photons, anywhere within the dressed state energy diagram. In addition, detuning Rabi frequencies increases the nutation frequency, which gives access to fast Rabi nutation speeds [16,17].

II. DETUNING REGIME MODEL

The $S = 5/2$ system of Mn^{2+} ions diluted in MgO has been extensively studied via electron paramagnetic resonance experiment (EPR) since it was first considered as a model for crystal field theory [18]. The Mn^{2+} ions are substituted for Mg^{2+} and have a cubic symmetry $F_{m\bar{3}m}$ (lattice constant 4.216 Å) ensuring that the spins see an almost isotropic crystalline environment. All the parameters of the crystal field and hyperfine interactions are known by independent studies. The spin Hamiltonian resolved by EPR is given by [18,19]

$$H = a/6\left[S_x^4 + S_y^4 + S_z^4 - S(S+1)(3S^2-1)/5\right] + \gamma\vec{H}_0\cdot\vec{S} - A\vec{S}\cdot\vec{I} + \gamma\vec{h}_{mw}\cdot\vec{S}\cos(2\pi f t), \quad (1)$$

where $\gamma = g\mu_B/h$ is the gyromagnetic ratio ($g = 2.0014$ the g factor, μ_B Bohr's magneton, and h Planck's constant), $S_{x,y,z}$ are the spin projection operators, $\vec{S}$ is the total spin, $a = 55.7$ MHz is the anisotropy constant, $A = 244$ MHz is the hyperfine constant of ^{55}Mn ($I = 5/2$), h_{mw} and f represent the microwave amplitude and frequency, respectively, and $\vec{H}_0$ is the static field ($\vec{H}_0 \perp \vec{h}_{mw}$). The applied static field ensures a Zeeman splitting of $\gamma H_0 \approx f \sim 9$ GHz, much stronger than all other interactions of Eq. (1). This implies that (i) $\vec{H}_0$'s direction can be approximated as the quantization axis and (ii) coherent microwave driving is confined between levels of same nuclear spin projection m_I (see also Refs. [6,20,21]). Consequently, the hyperfine interaction generates a constant field shift for all levels and it will be dropped from further analytical considerations (although it is part of the full numerical simulations).

Let us consider a quantum system with six states $|S_z\rangle$, $S_z = \{-5/2,-3/2,-1/2,1/2,3/2,5/2\}$, irradiated by an electromagnetic field. The spin Hamiltonian of the system is

$$\mathcal{H} = \hat{E} + \hat{V}(t) = \sum_{S_z=-5/2}^{5/2} E_{S_z}|S_z\rangle\langle S_z| + \hat{V}(t), \quad (2)$$

with E_{Sz} the static energy levels, $\hat{V}(t) = \frac{\gamma}{2}h_{mw}(\hat{S}_+ + \hat{S}_-)\cos(2\pi f t)$, and S_+/S_- the raising/lowering operators. Note that, contrary to our previous studies [12,22] where f was fixed to be in resonance with $1/2$ and $-1/2$ levels, here f is a free parameter. In a cubic symmetry and in first-order perturbation theory ($a \ll H_0$), the static energy levels are given by

$$\begin{aligned} E_{\pm5/2} &= (\pm5/2)\gamma H_0 + (1/2)pa + O(a^2), \\ E_{\pm3/2} &= (\pm3/2)\gamma H_0 - (3/2)pa + O(a^2), \\ E_{\pm1/2} &= (\pm1/2)\gamma H_0 + pa + O(a^2), \end{aligned} \quad (3)$$

where[18] $p = 1 - 5\sin^2\theta + \frac{15}{4}\sin^4\theta$ with θ the angle between $\vec{H}_0$ and the c axis [001]. Since $H_0 \gg h_{mw}$, we can use the rotating wave approximation (RWA) to make Eq. (2) time independent. We apply the unitary transformation

*sylvain.bertaina@im2np.fr

$U(t) = \exp(-i2\pi f \hat{S}_z t)$ and the Hamiltonian (2) becomes [14,20]

$$\mathcal{H}_{\mathrm{RWA}} = U\mathcal{H}U^{\dagger} + i\hbar\frac{\partial U}{\partial t}U^{\dagger} \tag{4}$$

$$= \begin{pmatrix} \frac{1}{2}pa - \frac{5}{2}\Delta & \frac{\sqrt{5}}{2}V & 0 & 0 & 0 & 0 \\ \frac{\sqrt{5}}{2}V & -\frac{3}{2}pa - \frac{3}{2}\Delta & \sqrt{2}V & 0 & 0 & 0 \\ 0 & \sqrt{2}V & pa - \frac{1}{2}\Delta & \frac{3}{2}V & 0 & 0 \\ 0 & 0 & \frac{3}{2}V & pa + \frac{1}{2}\Delta & \sqrt{2}V & 0 \\ 0 & 0 & 0 & \sqrt{2}V & -\frac{3}{2}pa + \frac{3}{2}\Delta & \frac{\sqrt{5}}{2}V \\ 0 & 0 & 0 & 0 & \frac{\sqrt{5}}{2}V & \frac{1}{2}pa + \frac{5}{2}\Delta \end{pmatrix}, \tag{5}$$

where $V = \gamma h_{mw}/2$ and Δ is the detuning parameter defined by $\Delta = f - (E_{1/2} - E_{-1/2})$. By diagonalization, the eigenenergies E_n/pa of the dressed states are calculated as a function of V and Δ. The Rabi frequency is the energy difference between two consecutive dressed states. Depending on the value of Δ, one can probe the "in-resonance one-photon process" ($\Delta = 0$), the "detuning-regime one-photon process" ($\Delta \neq 0$), and the "multiphoton process." The case $\Delta = 0$ has been reported in a previous study [12]. An example of the latter case, for which we discuss experimental evidence below, is $\Delta = \pm 5pa/4$ when two two-photon resonances occur.

In a typical pulsed EPR experiment there is only one frequency at a time available and the pulse sequence is composed of two parts: the spin manipulation and the probe sequence. Since the latter has to be at a frequency f in resonance with a one-photon transition, the experiment is restricted to be at $\Delta = 0$. In the current work, we use two microwave sources which allows us to manipulate any dressed state by using the first source f_1 and then probe the induced variation of populations using the second source f_2. A representation of the pulse sequence used for coherent manipulation in the case of a two-photon process is described in Fig. 1. To simplify the explanation only 3 out of 6 levels are shown. At $t = 0$, an oscillating field of frequency f_1 irradiates the system for a time τ_R. When the detuning Δ is such that the levels $|-1/2\rangle$ and $|3/2\rangle$ are separated by exactly $2hf_1$, a two-photon coherent transition is induced. To probe the populations of levels, a second pulse at frequency f_2 resonant with the transition between $|-1/2\rangle$ and $|1/2\rangle$ is sent at a time $t = \tau_p \gg T_2$ but smaller than T_1, where $T_{1,2}$ are the spin relaxation and decoherence times, respectively. This second pulse induces a free induced decay (FID) with an intensity proportional to the population difference $\sigma_{-1/2} - \sigma_{1/2}$ via a $\pi/2$ rotation in the subspace $S_z = \pm 1/2$.

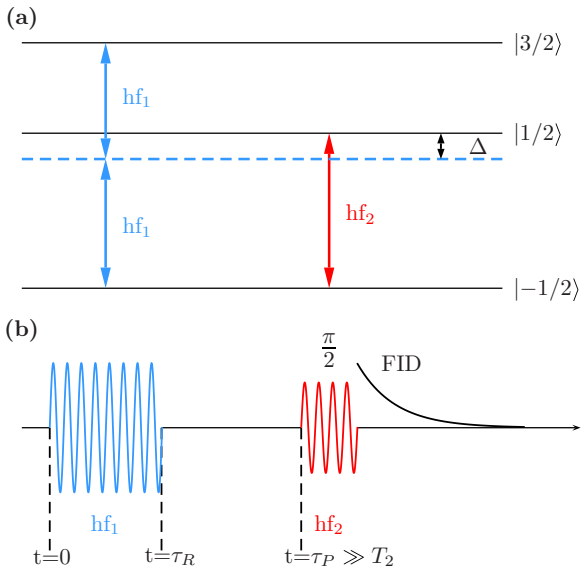

FIG. 1. (Color online) Representation of a two-photon pump and probe process. (a) Energy levels of Mn^{2+} [see Eq. (3)] for the subgroup $|\pm 1/2\rangle$ and $|3/2\rangle$. The arrows indicate the photon absorptions. The dashed line is a virtual level equidistant between $|-1/2\rangle$ and $|3/2\rangle$. (b) Pulse sequence: at $t = 0$ the microwave of frequency f_1 irradiates the spins and induces a Rabi nutation lasting up to $t = \tau_R$. To probe the population at the end of the first pulse, a second pulse at frequency f_2 in resonance with the transition between $|-1/2\rangle$ and $|1/2\rangle$ induces a $\pi/2$ rotation and thus an FID signal in the spectrometer.

III. EXPERIMENTAL PROCEDURE

The Rabi oscillation measurements were performed using a conventional Bruker Elexsys 680 pulse EPR spectrometer working at about 9.6 GHz. The second frequency source is provided by the ELDOR bridge of the spectrometer. To verify the reproducibility of the experiments, two different spectrometers using two different resonators, a dielectric (MD-5) and a split coil (MS-5), were used. The power-to-field conversion rate of the resonators is dependent on the frequency f_1 and it has been calibrated for all the frequencies used in this study using DPPH, an isotropic $S = 1/2$ system. The sample is a $(3\times3\times1)$-mm^3 single crystal of MgO doped by a small amount of Mn^{2+}.

A Rabi measurement consists of recording the FID intensity, as explained above, as a function of pulse length τ_R. Such Rabi oscillations are acquired for different excitation frequencies f_1, around the main one-photon Zeeman resonance f_2. Other important experimental parameters are the sample temperature and external field orientation (parameter p). In the current work, the temperature was set at 50 K which provides a long enough Rabi coherence time (~ 1 μs), while keeping the relaxation time sufficiently short to ensure a fast acquisition time [6,12]. Thus, the waiting time between the pump and probe pulses was set at 3 μs, larger than the decoherence time, but shorter than the relaxation time. The external field was oriented along the [111] axis of the crystal, ensuring a sizable

anharmonicity of the six-level system ($p = -2/3$) allowing the creation of virtual levels depicted by the dashed line in Fig. 1(b). It is important to note that the results described below are achievable in principle, for any orientation of the external field, the level anharmonicity being a tuning parameter $V/(pa)$ in such a multilevel quantum system.

IV. RESULTS AND DISCUSSION

After a Rabi oscillation is recorded, a Fourier transform indicates the Rabi frequency and its decay properties. An important aspect of our study relies on the possibility of detuning the excitation frequency f_1, as shown in the contour plot of Fig. 2(a). For moderate powers [$h_{mw} = 0.5(3)$ mT], one observes a fast one-photon branch (marked with "1") reaching Rabi flops of several tens of MHz. The branch shows a typical square-root law as a function of detuning [23] (see also Fig. 5). This technique allows for a significant speedup of electronic or nuclear spin Rabi frequencies [16,24,25] which are usually much slower than those achievable in superconducting qubits [26]. The quasienergies calculated as eigenenergies of Hamiltonian (5) are shown in Fig. 2(b) as a function of f_1. Crossings of the dashed lines (low-power case) indicate the location of resonances by crossovers, e.g., the one-, three-, and five-photon resonances at $\Delta = 0$ (discussed in our previous studies [6,12]). The labels in Fig. 2(b) indicate the number of photons involved in a given quasienergy crossing. We thus provide a method to reach any multiphoton resonance in the dressed state diagram by the use of detuning. Examples of such "resonances by detuning" are those labeled "2,3′,4". At the same time, by detuning away from such resonances, acceleration of their multiphoton Rabi frequency is observed, as indicated in Figs. 2(a) and 3(a) for each labeled resonance.

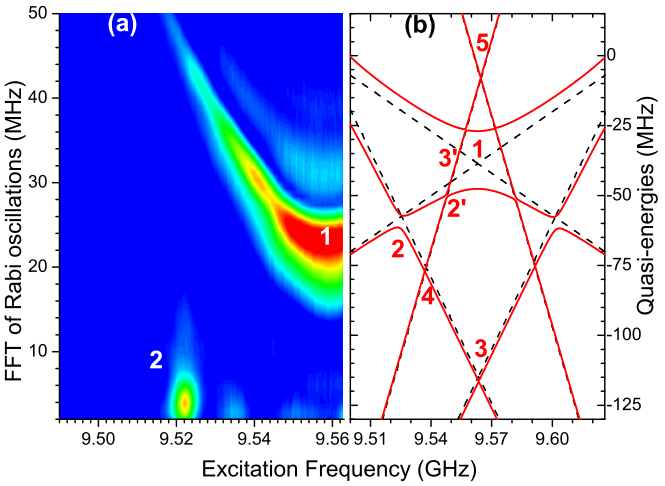

FIG. 2. (Color online) (a) Fourier transform of detuned Rabi oscillations measured at medium microwave power, $h_{mw} = 0.5(3)$ mT. The one-photon branch, marked with "1", can reach tens of MHz. An off-resonance two-photon branch, marked with "2", is also visible. The color map is in arbitrary units. (b) Quasienergies of Hamiltonian (5) calculated for low (dashed lines) and medium (continuous lines) microwave powers. The one-photon Rabi splitting (1) is excited when $f_1 = f_2$ while the two-photon transition (2) is at a detuned location given by Eq. (6).

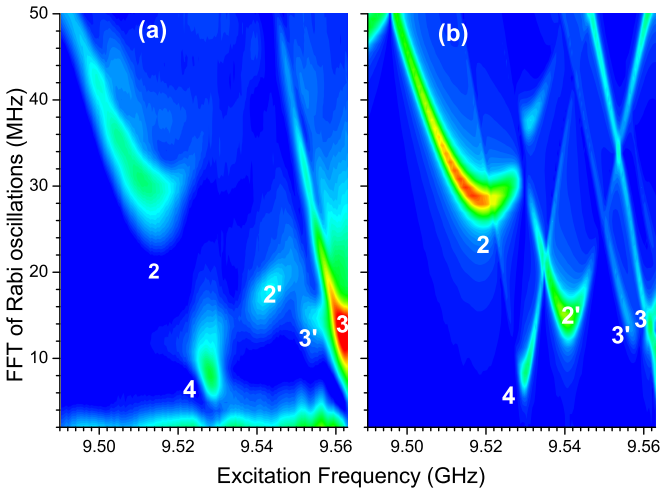

FIG. 3. (Color online) Measured (a) and simulated (b) Fourier transform of Rabi oscillations in the case of high microwave power [$h_{mw} = 1.7(8)$ mT]. The very good agreement allows identification of each Rabi splitting (shown in Fig. 2): two-photon (2 and 2′), three-photon (3 and 3′), and four-photon coherent rotations (4). The color map is in arbitrary units.

The continuous lines represent the eigenenergies calculated for the same power as the experimental data in Fig. 2. One observes the large one-photon splitting (1) which can be further accelerated by detuning (here, $f_1 < f_2$). A two-photon splitting of ∼4 MHz is visible as well (actual two-photon Rabi oscillations are shown in Fig. 4).

The Rabi splittings between consecutive quasienergies are strongly dependent on the microwave power. A Fourier

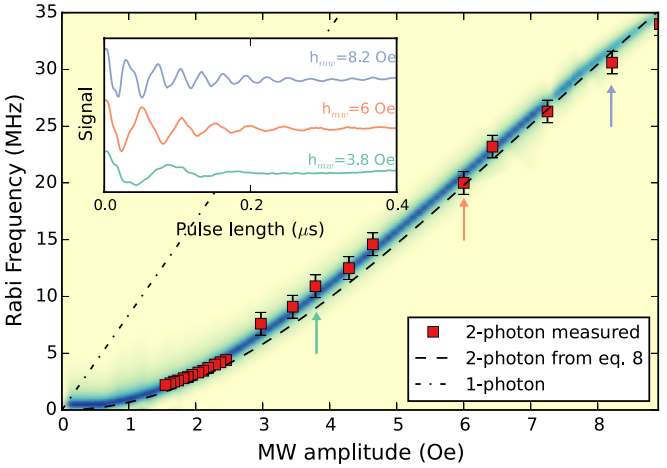

FIG. 4. (Color online) Microwave field dependence of two-photon coherent Rabi oscillations. The contour plot of the background is obtained via numerical simulations using the RWA (shade intensity in arbitrary units). The dashed line is given by Eq. (8) and it is in excellent agreement with the experimental values of the Rabi frequency (red squares). For comparison, the linear dependence of the one-photon Rabi frequency is shown by a dash-dotted line. Two-photon Rabi coherent oscillations are shown (insert) for three values of the microwave field, as indicated by small vertical arrows in the main panel.

transform contour plot for the high-power regime [$h_{mw} = 1.7(8)$ mT] is shown in Fig. 3: panel (a) shows experimental data while panel (b) shows numerical simulations based on exact diagonalization of Hamiltonian (1) after the RWA unitary transformation (4). One observes two two-photon coherent rotations (2 and 2′), two three-photon processes (3 and 3′), as well as four-photon detuned oscillations. The positions of these transitions as a function of detuning are visible in Fig. 2(b). The very good agreement between experiment and simulation allows the identification of all Rabi frequencies, and thus a predictable method of tuning level superposition between various S_z states of the Mn spin. Moreover, the possibility of frequency detuning between the control pulse f_1 and the $\pi/2$ readout pulse f_2 allows for selection of certain Rabi splittings without changing the external magnetic field. In the following, we demonstrate this protocol in the case of detuned two-photon coherent spin manipulation.

As discussed above, for $\Delta = -5pa/4$, one brings in resonance the levels $E_{1/2}$ and $E_{-3/2}$. Thus, the excitation frequency is given by

$$f_1 = \frac{1}{2}(E_{1/2} - E_{-3/2}) \tag{6}$$

and Hamiltonian (5) becomes

$$\mathcal{H}_{\mathrm{RWA}} = \begin{pmatrix} \frac{29}{8}pa & \frac{\sqrt{5}}{2}V & 0 & 0 & 0 & 0 \\ \frac{\sqrt{5}}{2}V & \frac{3}{8}pa & \sqrt{2}V & 0 & 0 & 0 \\ 0 & \sqrt{2}V & \frac{13}{8}pa & \frac{3}{2}V & 0 & 0 \\ 0 & 0 & \frac{3}{2}V & \frac{3}{8}pa & \sqrt{2}V & 0 \\ 0 & 0 & 0 & \sqrt{2}V & -\frac{27}{8}pa & \frac{\sqrt{5}}{2}V \\ 0 & 0 & 0 & 0 & \frac{\sqrt{5}}{2}V & -\frac{21}{8}pa \end{pmatrix} \tag{7}$$

showing the coupling between the diagonal elements $3pa/8$ via a two-photon process.

Taking $\tilde{h} = V/pa$ and restricting the analysis to low powers (keeping only terms quadratic in $\tilde{h}$), one finds that there is one eigenvalue $\epsilon = 3/8$. By looking for another eigenstate ϵ' close to 3/8 ($F_{\mathrm{Rabi}}^{2\mathrm{photon}} = \epsilon - \epsilon' \ll 1$), one can solve analytically for the Rabi frequency associated with this two-photon process,

$$F_{\mathrm{Rabi}}^{2\,\mathrm{photon}} = \frac{1902\tilde{h}^2}{585 + 713\tilde{h}^2}, \tag{8}$$

as a function of microwave power. This analytical relationship is in excellent agreement with experimental data (red squares), as shown in Fig. 4. The contour plot of the background is calculated using full diagonalization of the time-dependent Schrödinger equation, while the dashed line is given by Eq. (8), with no fit parameters. The linear microwave field dependence of a one-photon Rabi frequency is given as dash-dotted line, as a comparison. The inset shows actual two-photon Rabi oscillations for three values of the microwave field, as indicated by the small vertical arrows in the main panel. These measurements are done at the two-photon resonance [marked with "2" in Fig. 2(b)] by properly detuning f_1 with respect to f_2.

One can also study the effect of the detuning away from a particular Rabi resonance. We record spin oscillations for

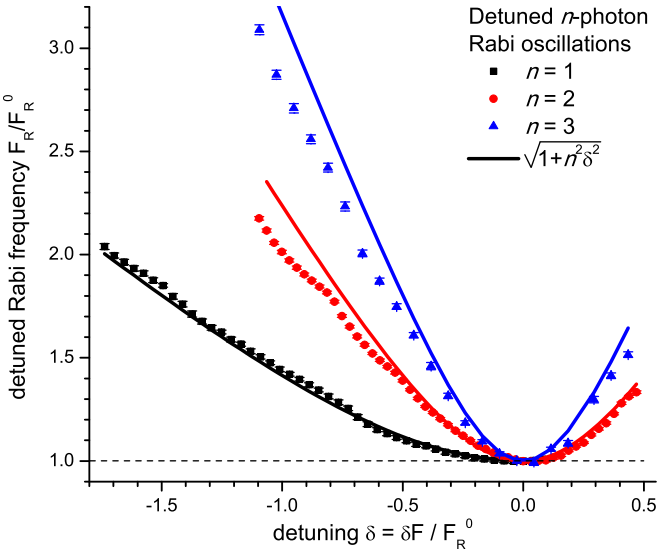

FIG. 5. (Color online) Acceleration of n-photon Rabi frequencies as a function of detuning. Experimental data are shown by black squares (one-photon), red dots (two-photon), and blue triangles (three-photon Rabi splittings), while the continuous lines are calculated from Eq. (9).

value of f_1 around Rabi splittings corresponding to one-, two- and three-photon processes [marked with "1", "2", and "3", respectively, in Fig. 2(b)]. Their Fourier transform give the values of the Rabi splittings, as plotted in Fig. 5. The obtained frequencies follow very well a generalized Rabi formula for n photons, given by

$$F_R = \sqrt{\left(F_R^0\right)^2 + n^2\delta F^2}, \tag{9}$$

where F_R^0 is the Rabi frequency at resonance, n is the number of photons responsible for the coherent drive, and δF is the detuning away from a Rabi resonance. For instance, in the case of the two-photon coherent oscillations, $n = 2$, $F_R^0 = F_{\mathrm{Rabi}}^{2\,\mathrm{photon}}$ of Eq. (8) and the detuning is the shift of f_1 away from the splitting marked "2" in Fig. 2(b). For one photon, the above equation is reduced to the well-known Rabi formula [23]. This observed acceleration of the Rabi flops due to detuning can be an important tool to achieve fast operation of spin qubits [16].

V. CONCLUSION

In conclusion, we demonstrate a pulse technique allowing for coherent operation of multiphoton Rabi oscillations through detuning. Two microwave pulses are detuned such that one excites with a specified number of photons while the other one provides the readout at the single-photon resonance. The technique allows for a significant speedup of Rabi nutation by detuning the one- or multiphoton coherent rotation. The provided analytical and numerical methods allows for a well-defined control and tuning of the spin dynamics in this multilevel solid state system.

ACKNOWLEDGMENTS

This work was supported by NSF Grant No. DMR-1206267, CNRS-PICS CoDyLow, and CNRS's research federation RENARD (FR3443) for EPR facilities. The NHMFL is supported by Cooperative Agreement Grant No. DMR-1157490 and the state of Florida.

[1] S. Nellutla, K.-Y. Choi, M. Pati, J. van Tol, I. Chiorescu, and N. S. Dalal, Coherent manipulation of electron spins up to ambient temperatures in $Cr^{5+}(S = 1/2)$ doped K_3NbO_8, Phys. Rev. Lett. **99**, 137601 (2007).

[2] M. V. G. Dutt, L. Childress, L. Jiang, E. Togan, J. Maze, F. Jelezko, A. S. Zibrov, P. R. Hemmer, and M. D. Lukin, Quantum register based on individual electronic and nuclear spin qubits in diamond, Science **316**, 1312 (2007).

[3] S. Bertaina, S. Gambarelli, A. Tkachuk, I. N. Kurkin, B. Malkin, A. Stepanov, and B. Barbara, Rare-earth solid-state qubits, Nat. Nanotechnol. **2**, 39 (2007).

[4] A. Ardavan, O. Rival, J. J. L. Morton, S. J. Blundell, A. M. Tyryshkin, G. A. Timco, and R. E. P. Winpenny, Will spin-relaxation times in molecular magnets permit quantum information processing?, Phys. Rev. Lett. **98**, 057201 (2007).

[5] S. Bertaina, S. Gambarelli, T. Mitra, B. Tsukerblat, A. Müller, and B. Barbara, Quantum oscillations in a molecular magnet., Nature (London) **453**, 203 (2008).

[6] S. Bertaina, L. Chen, N. Groll, J. Van Tol, N. S. Dalal, and I. Chiorescu, Multiphoton coherent manipulation in large-spin qubits, Phys. Rev. Lett. **102**, 050501 (2009).

[7] F. Jelezko, T. Gaebel, I. Popa, A. Gruber, and J. Wrachtrup, Observation of coherent oscillations in a single electron spin, Phys. Rev. Lett. **92**, 076401 (2004).

[8] I. Chiorescu, N. Groll, S. Bertaina, T. Mori, and S. Miyashita, Magnetic strong coupling in a spin-photon system and transition to classical regime, Phys. Rev. B **82**, 024413 (2010).

[9] Y. Kubo, F. R. Ong, P. Bertet, D. Vion, V. Jacques, D. Zheng, A. Dréau, J.-F. Roch, A. Auffeves, F. Jelezko, J. Wrachtrup, M. F. Barthe, P. Bergonzo, and D. Esteve, Strong coupling of a spin ensemble to a superconducting resonator, Phys. Rev. Lett. **105**, 140502 (2010).

[10] D. I. Schuster, A. P. Sears, E. Ginossar, L. DiCarlo, L. Frunzio, J. J. L. Morton, H. Wu, G. A. D. Briggs, B. B. Buckley, D. D. Awschalom, and R. J. Schoelkopf, High-cooperativity coupling of electron-spin ensembles to superconducting cavities, Phys. Rev. Lett. **105**, 140501 (2010).

[11] M. Blencowe, Quantum computing quantum ram, Nature (London) **468**, 44 (2010).

[12] S. Bertaina, N. Groll, L. Chen, and I. Chiorescu, Tunable multiphoton rabi oscillations in an electronic spin system, Phys. Rev. B **84**, 134433 (2011).

[13] M. N. Leuenberger and D. Loss, Quantum computing in molecular magnets, Nature (London) **410**, 789 (2001).

[14] M. N. Leuenberger and D. Loss, Grover algorithm for large nuclear spins in semiconductors, Phys. Rev. B **68**, 165317 (2003).

[15] M. Grace, C. Brif, H. Rabitz, I. Walmsley, R. Kosut, and D. Lidar, Encoding a qubit into multilevel subspaces, New J. Phys. **8**, 35 (2006).

[16] J. Yoneda, T. Otsuka, T. Nakajima, T. Takakura, T. Obata, M. Pioro-Ladrière, H. Lu, C. J. Palmstrøm, A. C. Gossard, and S. Tarucha, Fast electrical control of single electron spins in quantum dots with vanishing influence from nuclear spins, Phys. Rev. Lett. **113**, 267601 (2014).

[17] S. Chesi, Y.-D. Wang, J. Yoneda, T. Otsuka, S. Tarucha, and D. Loss, Single-spin manipulation in a double quantum dot in the field of a micromagnet, Phys. Rev. B **90**, 235311 (2014).

[18] W. Low, Paramagnetic resonance spectrum of manganese in cubic MgO and CaF_2, Phys. Rev. **105**, 793 (1957).

[19] S. R. P. Smith, P. V. Auzins, and J. E. Wertz, Angular dependence of the intensities of "forbidden" transitions of Mn^{2+} in MgO, Phys. Rev. **166**, 222 (1968).

[20] C. Hicke and M. I. Dykman, Multiphoton antiresonance in large-spin systems, Phys. Rev. B **76**, 054436 (2007).

[21] A. Schweiger and G. Jeschke, *Principles of Pulse Electron Paramagnetic Resonance* (Oxford University Press, Oxford, 2001).

[22] S. Bertaina, J. H. Shim, S. Gambarelli, B. Z. Malkin, and B. Barbara, Spin-orbit qubits of rare-earth-metal ions in axially symmetric crystal fields, Phys. Rev. Lett. **103**, 226402 (2009).

[23] C. Cohen-Tannoudji, B. Diu, and F. Laloë, *Quantum Mechanics* (Hermann, Paris, 1973).

[24] S. Rohr, E. Dupont-Ferrier, B. Pigeau, P. Verlot, V. Jacques, and O. Arcizet, Synchronizing the dynamics of a single nitrogen vacancy spin qubit on a parametrically coupled radio-frequency field through microwave dressing, Phys. Rev. Lett. **112**, 010502 (2014).

[25] C. Avinadav, R. Fischer, P. London, and D. Gershoni, Time-optimal universal control of two-level systems under strong driving, Phys. Rev. B **89**, 245311 (2014).

[26] I. Chiorescu, P. Bertet, K. Semba, Y. Nakamura, C. J. P. M. Harmans, and J. E. Mooij, Coherent dynamics of a flux qubit coupled to a harmonic oscillator, Nature (London) **431**, 159 (2004).